Electronic Supplementary Material (ESI) for Journal of Materials Chemistry A.

Electronic Supplementary Information of Theoretical study of the mechanism for photocatalytic CO_2 reduction to methanol over layered double hydroxides

Si-Min Xu,*[a] Rui Xu,[b] Yu-Quan Zhu,[c] Ling Zhu [a] and Yingtong Zong*[a]

[a.] *College of Chemistry and Chemical Engineering, Gannan Normal University, Ganzhou, 341000, P. R. China. E-mail: xusimin@gnnu.edu.cn (S.-M. Xu), zongyingtong@gnnu.edu.cn (Y. Zong).*

[b.] *Jiangxi Intellectual Property Protection Center, Nanchang, 330006, P. R. China.*

[c.] *Hubei Key Laboratory of Pollutant Analysis & Reuse Technology, College of Chemistry and Chemical Engineering, Hubei Normal University, Huangshi, 435002, P. R. China.*

Contents

Notes

Note 1

In our previous work, we have found that the lattice parameters of LDHs are influenced by the external stress set during geometry optimization (*J. Mater. Chem. A*, 2021, **9**, 20466–20482). In general, the lattice parameters *a*, *b*, and *c* decrease with the increasing external stress. In this work, a benchmark test of external stress was performed on Mg_2Al-NO_3-LDH. Mg_2Al-NO_3-LDH was optimized under the external stress of 0.1 – 10.0 GPa with a step length of 0.1 GPa. The lattice parameters *c*, which is more sensitive to external stress than *a* and *b*, matches well with the experimental value under the external stress of 3.8 GPa (*Catal. Today*, 1991, **11**, 173–301). Therefore, the external stress of 3.8 GPa is applied in this work.

Note 2

In order to obtain an accurate work function of M_2M'-NO_3-LDH, the number of bilayers for LDHs and thickness of vacuum layer need to be properly set. Firstly, we performed benchmark calculations on the number of bilayers for Mg_2Al-NO_3-LDH. The vacuum layer was set to be 120 Å. The values of work functions for Mg_2Al-NO_3-LDH with different bilayers were calculated to be 4.738, 4.682, 4.679, 4.850, 4.811, and 4.721 eV for one, two, three, four, five, and six bilayers, respectively, as shown in Fig. S1. The work function of Mg_2Al-NO_3-LDH with only one bilayer (4.738 eV) is close to that with six bilayers (4.721 eV). This result is different from that for metal or metal oxide. Although this result is surprising at first impression, but can be well understood. Unlike metal or metal oxide binding with metal bond or covalent bond, the interaction between LDH matrix and interlayer guest is mainly Coulomb force, and van der Waals force, which is much weaker than covalent bond. Thus the electronic structure of LDH matrix is not severely influenced by the interaction between LDH bilayers. Therefore, the work function of LDH can be well represented by LDH with one bilayer.

On the other hand, we calculated the work functions of Mg_2Al-NO_3-LDH (003) surface (one bilayer) with the thickness of vacuum layer ranging from 20 to 160 Å. As is shown in Fig. S2, the work function of Mg_2Al-NO_3-LDH (003) surface is not converged when the thickness of vacuum layer is smaller than 70 Å. The work function of Mg_2Al-NO_3-LDH (003) surface with the thickness of vacuum layer of 70 Å is only 0.034 eV larger than that with a vacuum layer as thick as 120 Å. Therefore, a vacuum layer with the thickness of 70 Å is sufficient for accurately calculating the work function of LDH (003) surface.

Note 3

In order to determine the cutoff energy employed in this work, the cutoff energies of both 400 eV and 600 eV were applied to calculate the Gibbs free energy changes (ΔG) of elementary steps in CO_2 reduction over Mg_2Al-NO_3-LDH. The average absolute value of deviation between ΔG obtained by 400 eV and that by 600 eV was calculated to be 0.09 eV, which is smaller than 0.1 eV. Therefore, we believe that a cutoff energy of 400 eV is accurate enough and cost-effective.

Note 4

In order to determine the *k*-point meshes employed in this work, the *k*-point meshes of both 3 × 3 × 1 and 5 × 5 × 1 were applied to calculate the Gibbs free energy changes (ΔG) of elementary steps in CO_2 reduction over Mg_2Al-NO_3-LDH. The average absolute value of deviation between ΔG obtained by 3 × 3 × 1 and that by 5 × 5 × 1 was calculated to be 0.09 eV, which is smaller than 0.1 eV. Therefore, we believe that a *k*-point meshes of 3 × 3 × 1 is accurate enough and cost-effective.

Note 5

The photocatalytic driving force E_{df} is identified as the difference between the ΔG in the condition of standard hydrogen electrode (ΔG_{SHE}) and the ΔG under reaction condition ($\Delta G_{Reaction}$), i.e., $E_{df} = \Delta G_{SHE} - \Delta G_{Reaction}$. Then, the following equation can be obtained:

$$
\begin{aligned}
&E_{df} \\
&= \Delta G_{SHE} - \Delta G_{Reaction} \\
&= (G_{\text{product in the condition of SHE}} - G_{\text{reactant in the condition of SHE}}) - (G_{\text{product in reaction condition}} - G_{\text{reactant in reaction condition}})
\end{aligned}
$$

Given that only the Gibbs free energies of H^+ and e^- are different in the condition of standard hydrogen electrode and in reaction condition, the equation can be simplified as follows:

$$
\begin{aligned}
&E_{df} \\
&= G_{(H^+ + e^-)\text{ in reaction condition}} - G_{(H^+ + e^-)\text{ in the condition of SHE}} \\
&= (G_{H^+\text{ in reaction condition}} - G_{H^+\text{ in the condition of SHE}}) + (G_{e^-\text{ in reaction condition}} - G_{e^-\text{ in the condition of SHE}}) \\
&= (G_{H^+\text{ in pH 7}} - G_{H^+\text{ in pH 0}}) + (G_{e^-\text{ in CBM}} - (-4.5\,\text{eV})) \\
&= -kT\ln 10\Delta\text{pH} + E_{CBM} + 4.5\,\text{eV} \\
&= E_{CBM} + 4.09\,\text{eV}
\end{aligned}
$$

Figures

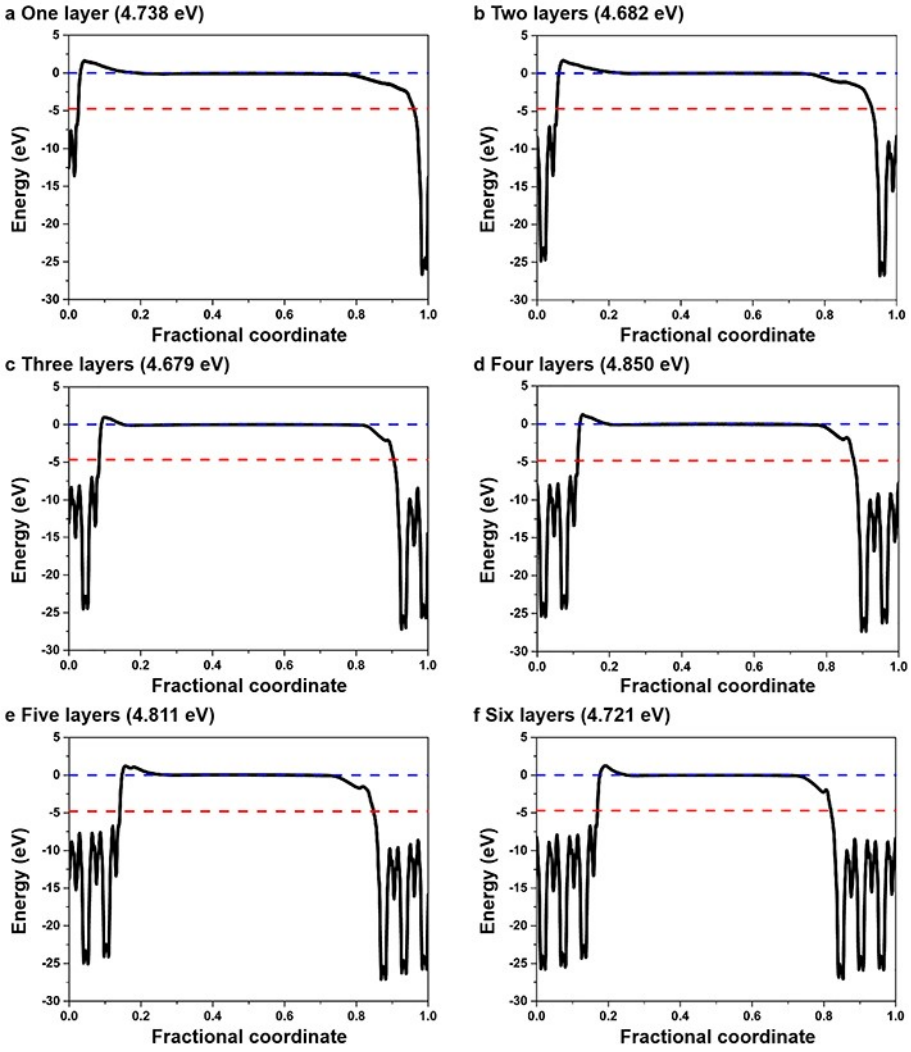

Fig. S1 Work functions of the (001) surfaces for Mg_2Al-NO_3-LDH with (a) one layer, (b) two layers, (c) three layers, (d) four layers, (e) five layers, and (f) six layers, respectively. Vacuum level (set as zero point) and Fermi level are labeled with dashed blue line and red line, respectively. Value of the work function is listed in the bracket.

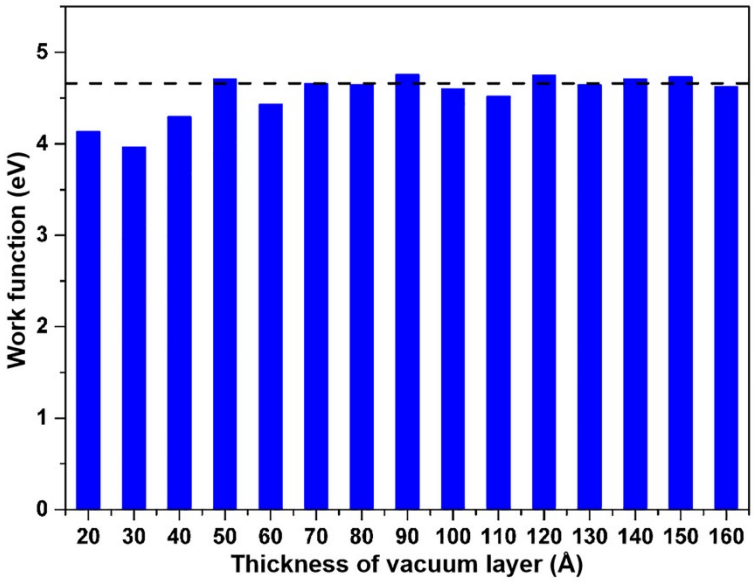

Fig. S2 Work functions of Mg_2Al-NO_3-LDH with one bilayer and vacuum layer with different thickness.

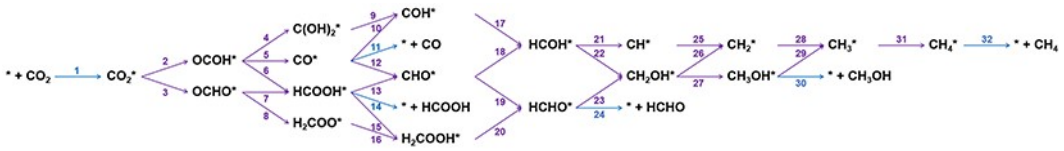

Fig. S3 Main elementary steps in CO_2 reduction to CO, HCOOH, HCHO, CH_3OH, and CH_4. Blue arrows represent adsorption and desorption steps and purple arrows represent reduction steps.

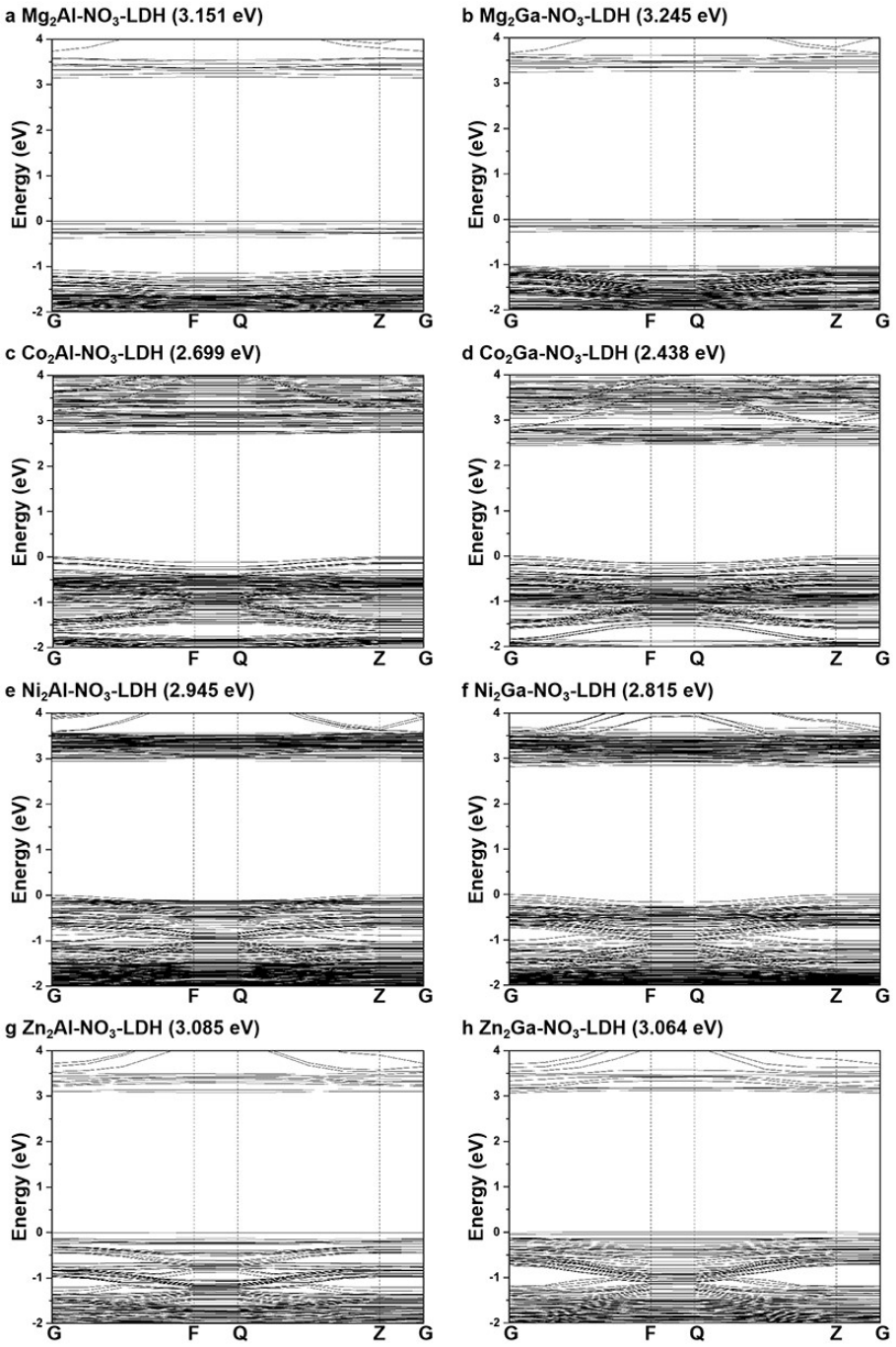

Fig. S4 Band structures of (a) Mg_2Al-NO_3-LDH, (b) Mg_2Ga-NO_3-LDH, (c) Co_2Al-NO_3-LDH, (d) Co_2Ga-NO_3-LDH, (e) Ni_2Al-NO_3-LDH, (f) Ni_2Ga-NO_3-LDH, (g) Zn_2Al-NO_3-LDH, and (h) Zn_2Ga-NO_3-LDH. The band gap energy of each M_2M'-NO_3-LDH is listed in the bracket.

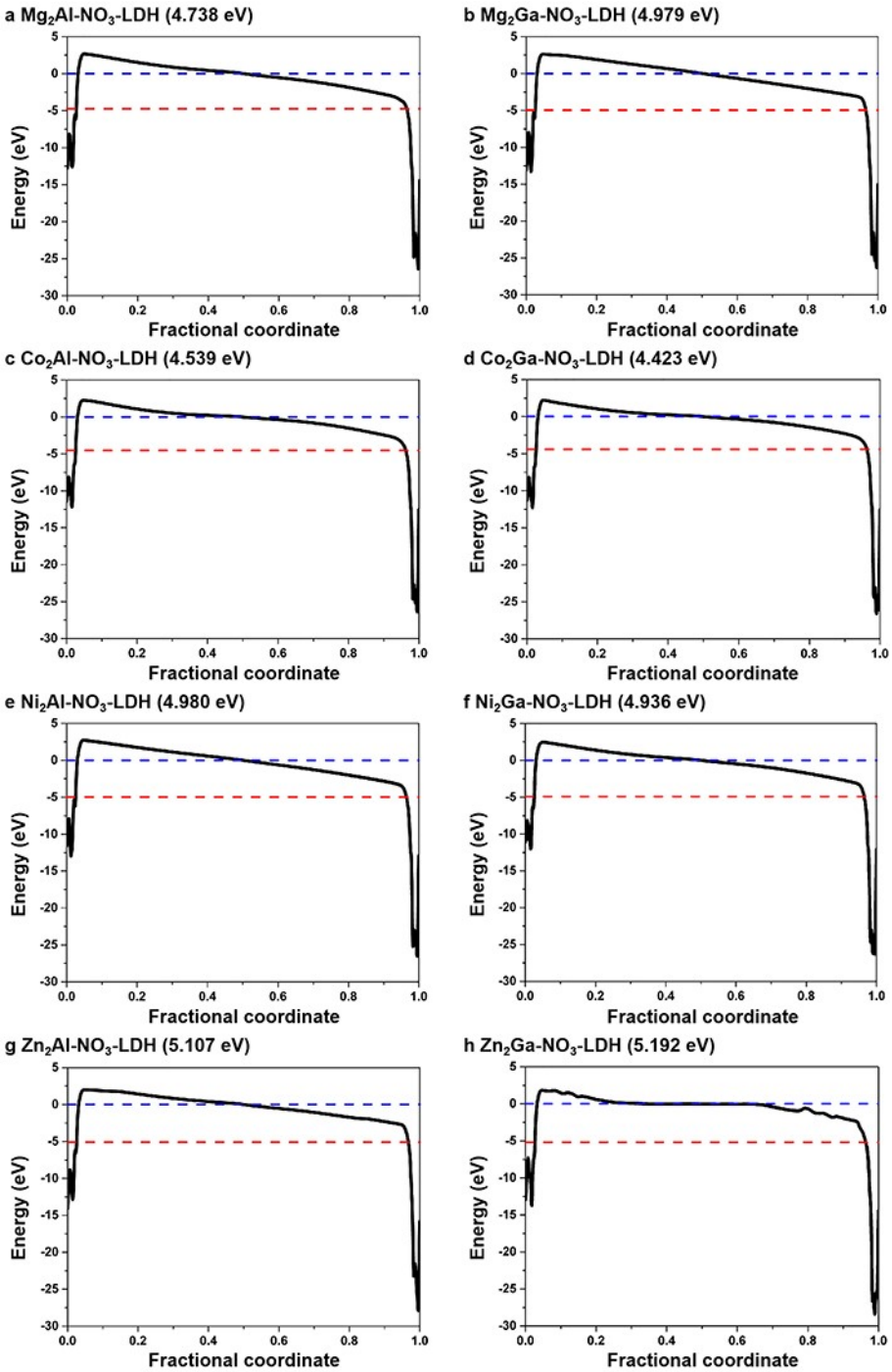

Fig. S5 Work functions of the (001) surfaces for (a) Mg_2Al-NO_3-LDH, (b) Mg_2Ga-NO_3-LDH, (c) Co_2Al-NO_3-LDH, (d) Co_2Ga-NO_3-LDH, (e) Ni_2Al-NO_3-LDH, (f) Ni_2Ga-NO_3-LDH, (g) Zn_2Al-NO_3-LDH, and (h) Zn_2Ga-NO_3-LDH, respectively. Vacuum level (set as zero point) and Fermi level are labeled with dashed blue line and red line, respectively. Value of the work function is listed in the bracket.

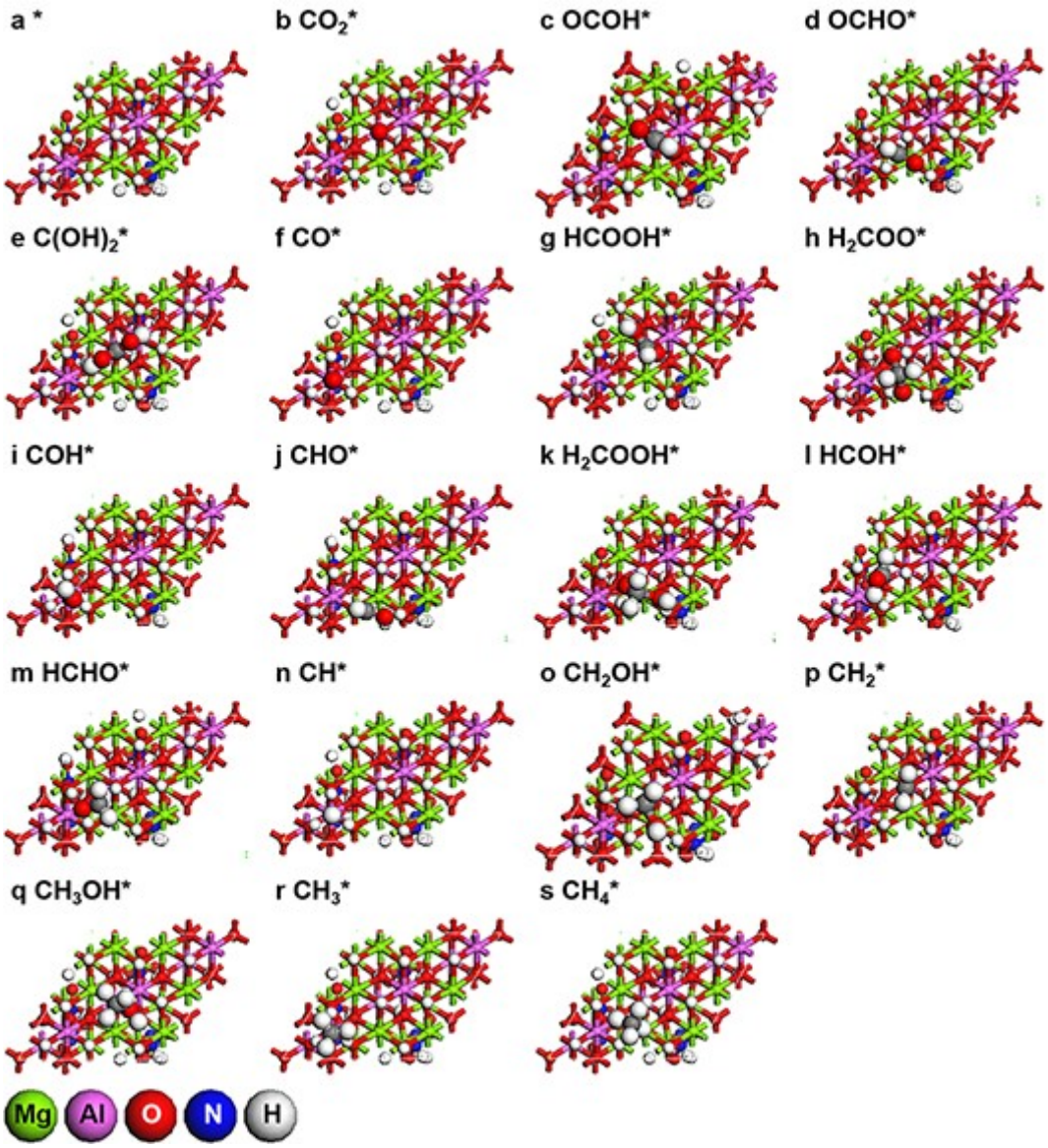

Fig. S6 Optimized geometries of reaction intermediates during CO_2 reduction over Mg_2Al-NO_3-LDH: (a) *, (b) CO_2*, (c) OCOH*, (d) OCHO*, (e) $C(OH)_2$*, (f) CO*, (g) HCOOH*, (h) H_2COO*, (i) COH*, (j) CHO*, (k) H_2COOH*, (l) HCOH*, (m) HCHO*, (n) CH*, (o) CH_2OH*, (p) CH_2*, (q) CH_3OH*, (r) CH_3*, and (s) CH_4*, respectively. The color code of each element is displayed on the bottom.

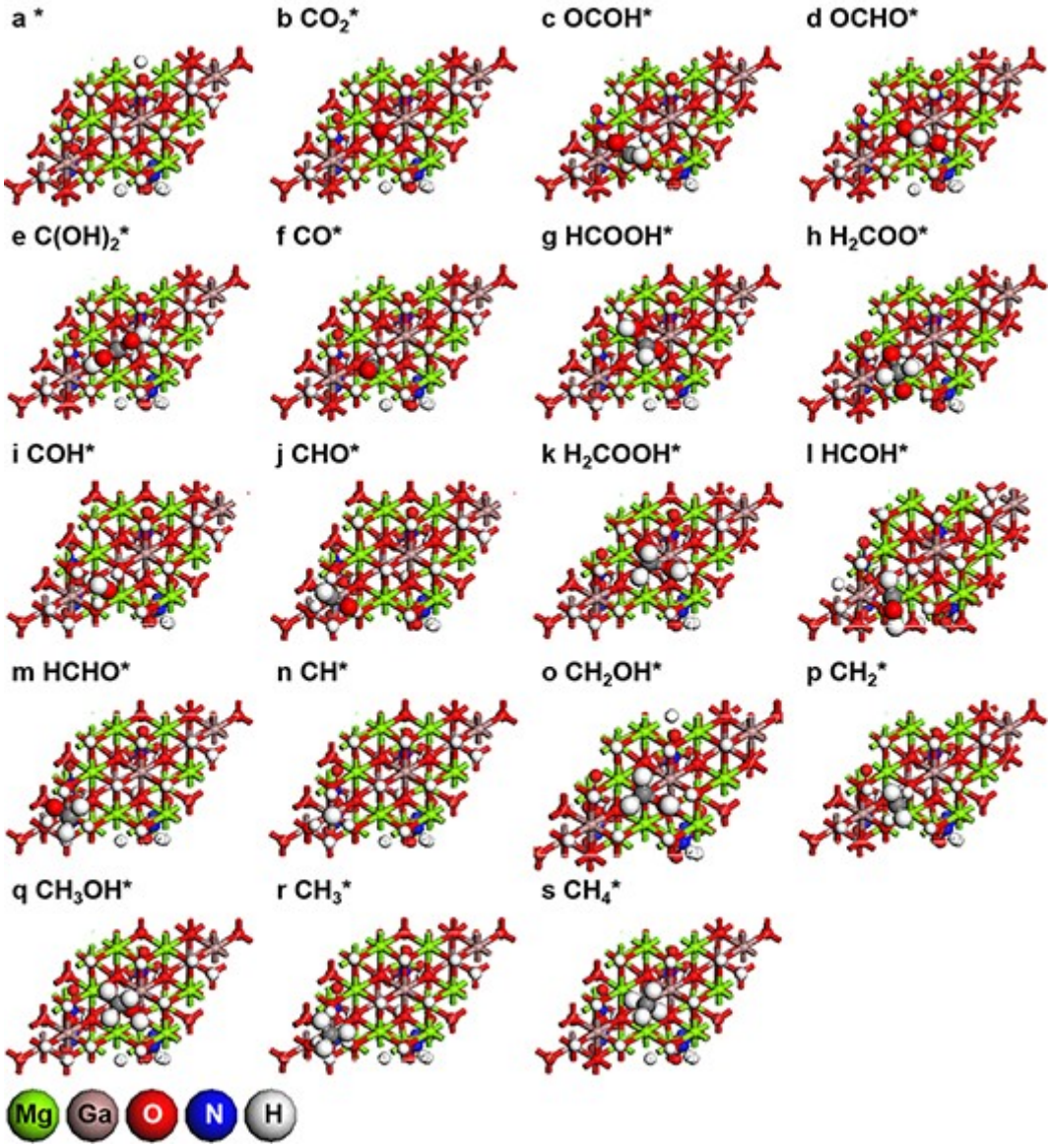

Fig. S7 Optimized geometries of reaction intermediates during CO_2 reduction over Mg_2Ga-NO_3-LDH: (a) *, (b) CO_2*, (c) OCOH*, (d) OCHO*, (e) $C(OH)_2$*, (f) CO*, (g) HCOOH*, (h) H_2COO*, (i) COH*, (j) CHO*, (k) H_2COOH*, (l) HCOH*, (m) HCHO*, (n) CH*, (o) CH_2OH*, (p) CH_2*, (q) CH_3OH*, (r) CH_3*, and (s) CH_4*, respectively. The color code of each element is displayed on the bottom.

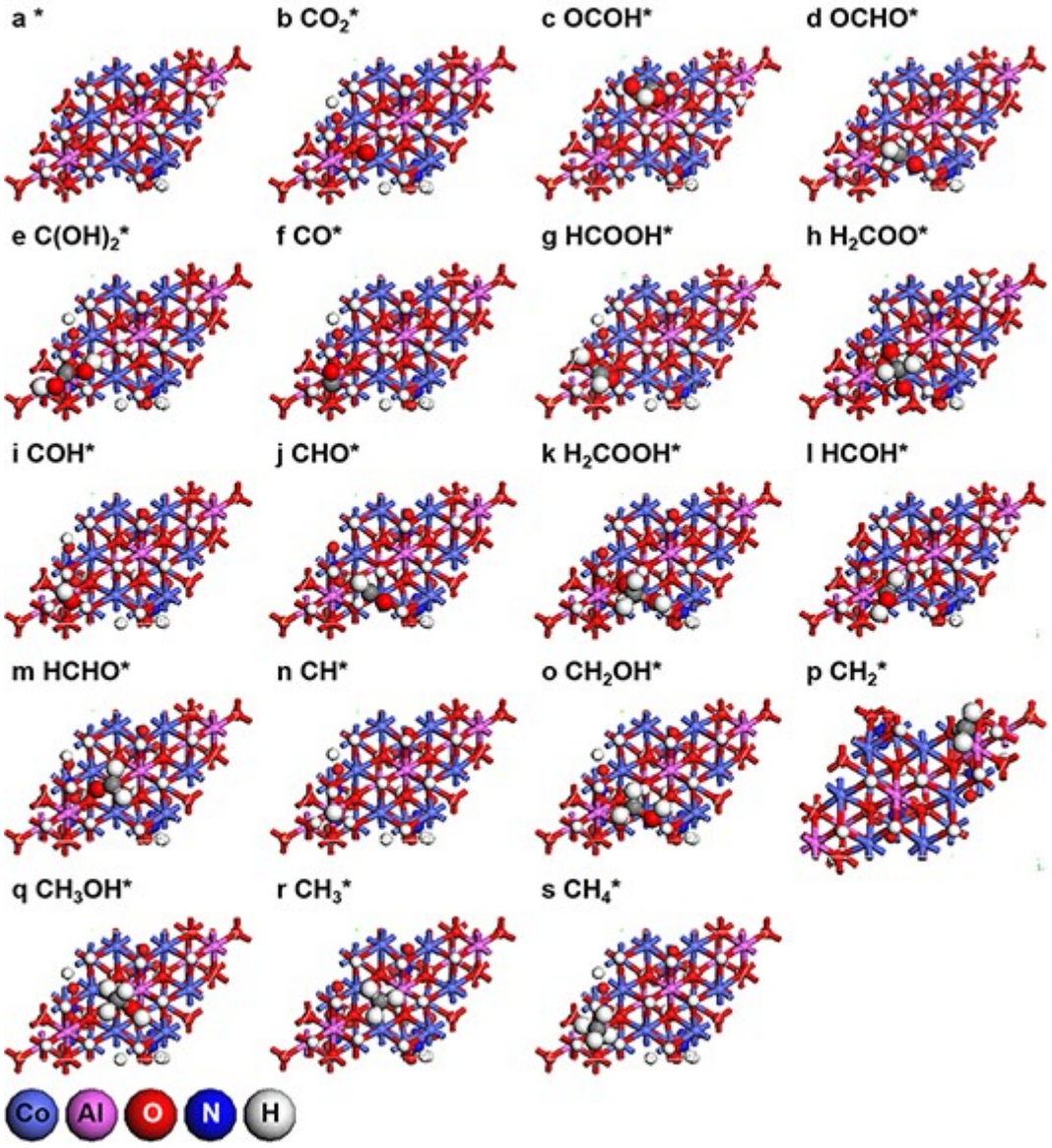

Fig. S8 Optimized geometries of reaction intermediates during CO_2 reduction over Co_2Al-NO_3-LDH: (a) *, (b) CO_2*, (c) OCOH*, (d) OCHO*, (e) $C(OH)_2$*, (f) CO*, (g) HCOOH*, (h) H_2COO*, (i) COH*, (j) CHO*, (k) H_2COOH*, (l) HCOH*, (m) HCHO*, (n) CH*, (o) CH_2OH*, (p) CH_2*, (q) CH_3OH*, (r) CH_3*, and (s) CH_4*, respectively. The color code of each element is displayed on the bottom.

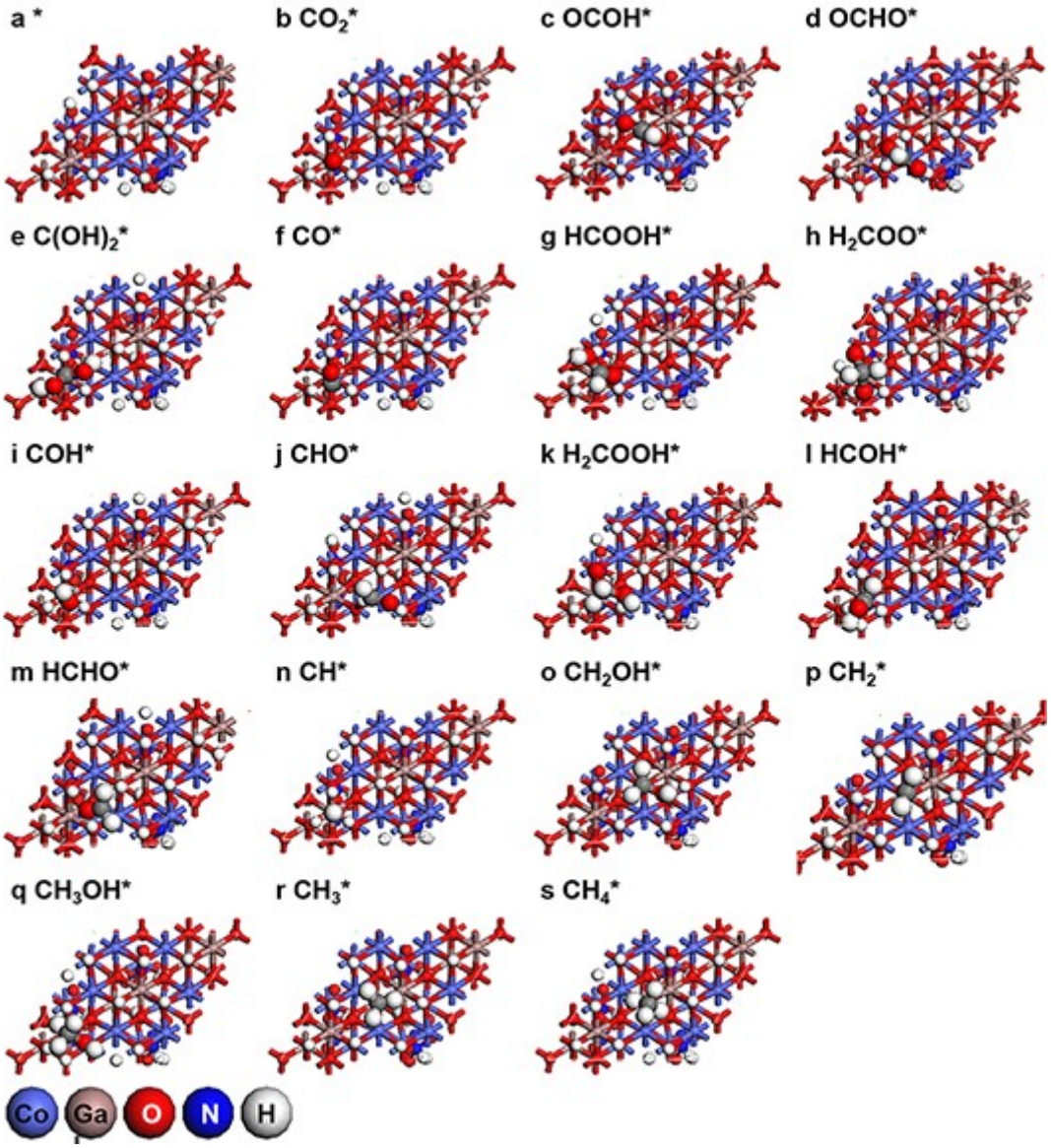

Fig. S9 Optimized geometries of reaction intermediates during CO_2 reduction over Co_2Ga-NO_3-LDH: (a) *, (b) CO_2*, (c) OCOH*, (d) OCHO*, (e) $C(OH)_2$*, (f) CO*, (g) HCOOH*, (h) H_2COO*, (i) COH*, (j) CHO*, (k) H_2COOH*, (l) HCOH*, (m) HCHO*, (n) CH*, (o) CH_2OH*, (p) CH_2*, (q) CH_3OH*, (r) CH_3*, and (s) CH_4*, respectively. The color code of each element is displayed on the bottom.

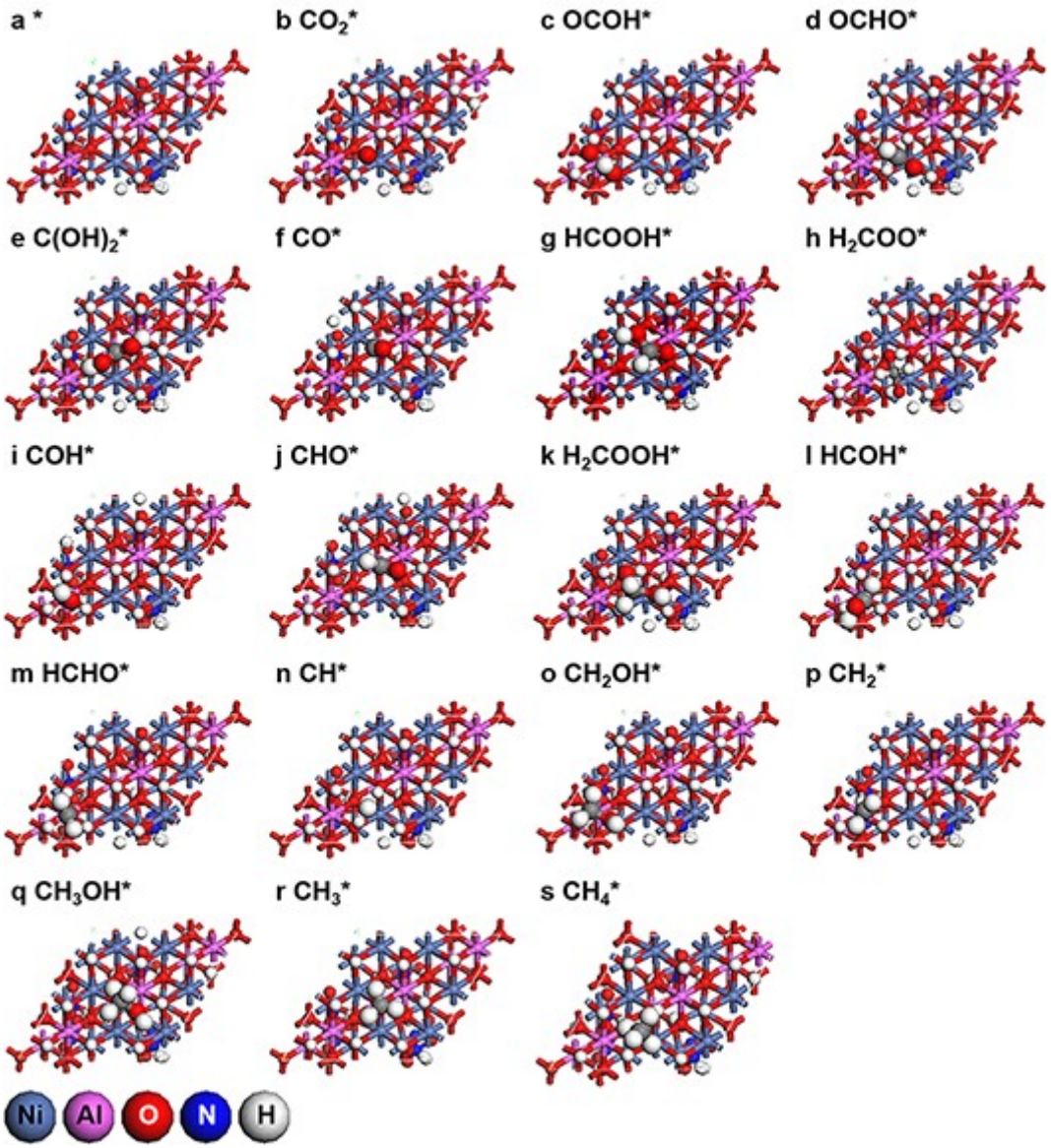

Fig. S10 Optimized geometries of reaction intermediates during CO_2 reduction over Ni_2Al-NO_3-LDH: (a) *, (b) CO_2*, (c) OCOH*, (d) OCHO*, (e) $C(OH)_2$*, (f) CO*, (g) HCOOH*, (h) H_2COO*, (i) COH*, (j) CHO*, (k) H_2COOH*, (l) HCOH*, (m) HCHO*, (n) CH*, (o) CH_2OH*, (p) CH_2*, (q) CH_3OH*, (r) CH_3*, and (s) CH_4*, respectively. The color code of each element is displayed on the bottom.

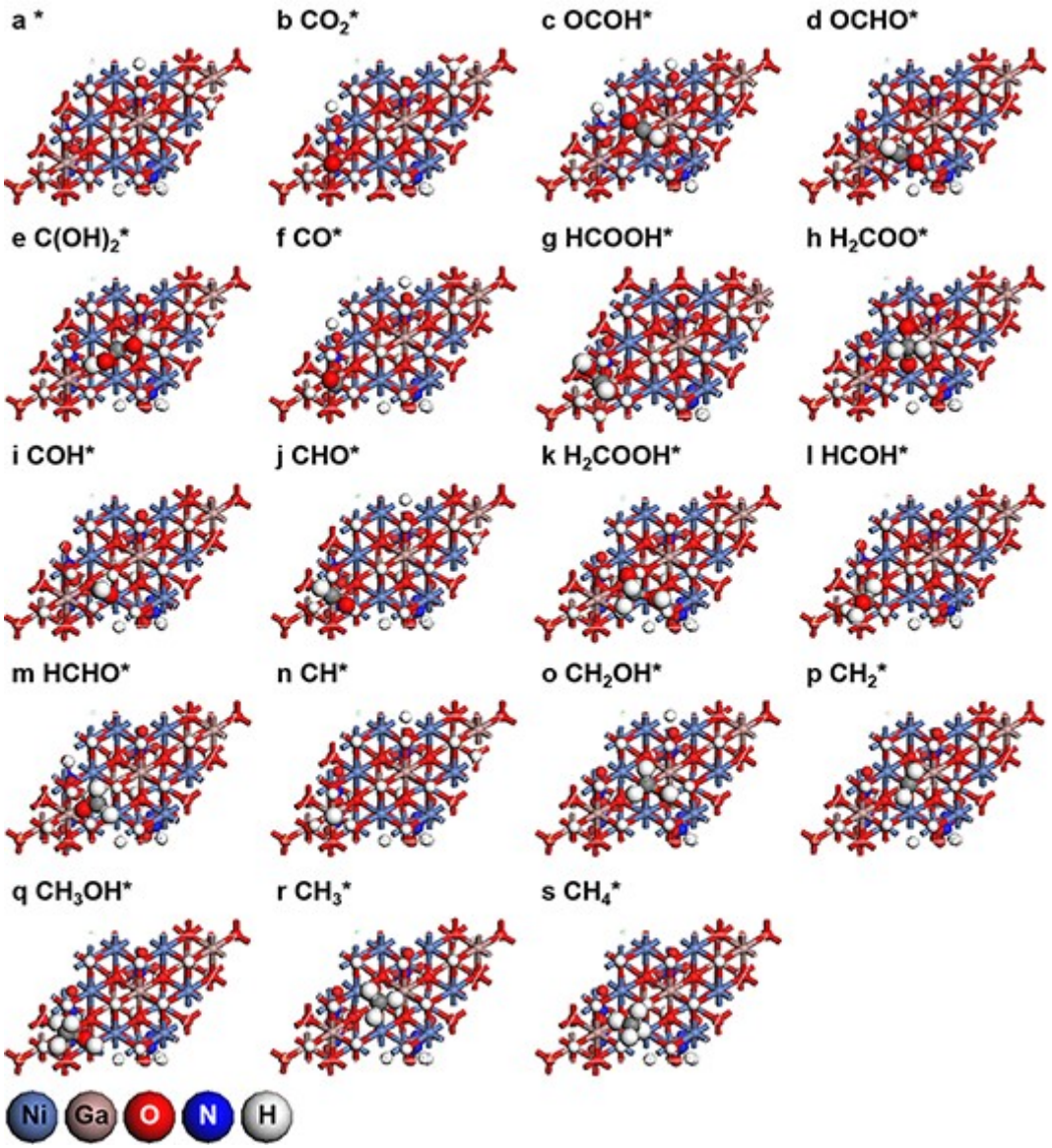

Fig. S11 Optimized geometries of reaction intermediates during CO_2 reduction over Ni_2Ga-NO_3-LDH: (a) *, (b) CO_2*, (c) OCOH*, (d) OCHO*, (e) $C(OH)_2$*, (f) CO*, (g) HCOOH*, (h) H_2COO*, (i) COH*, (j) CHO*, (k) H_2COOH*, (l) HCOH*, (m) HCHO*, (n) CH*, (o) CH_2OH*, (p) CH_2*, (q) CH_3OH*, (r) CH_3*, and (s) CH_4*, respectively. The color code of each element is displayed on the bottom.

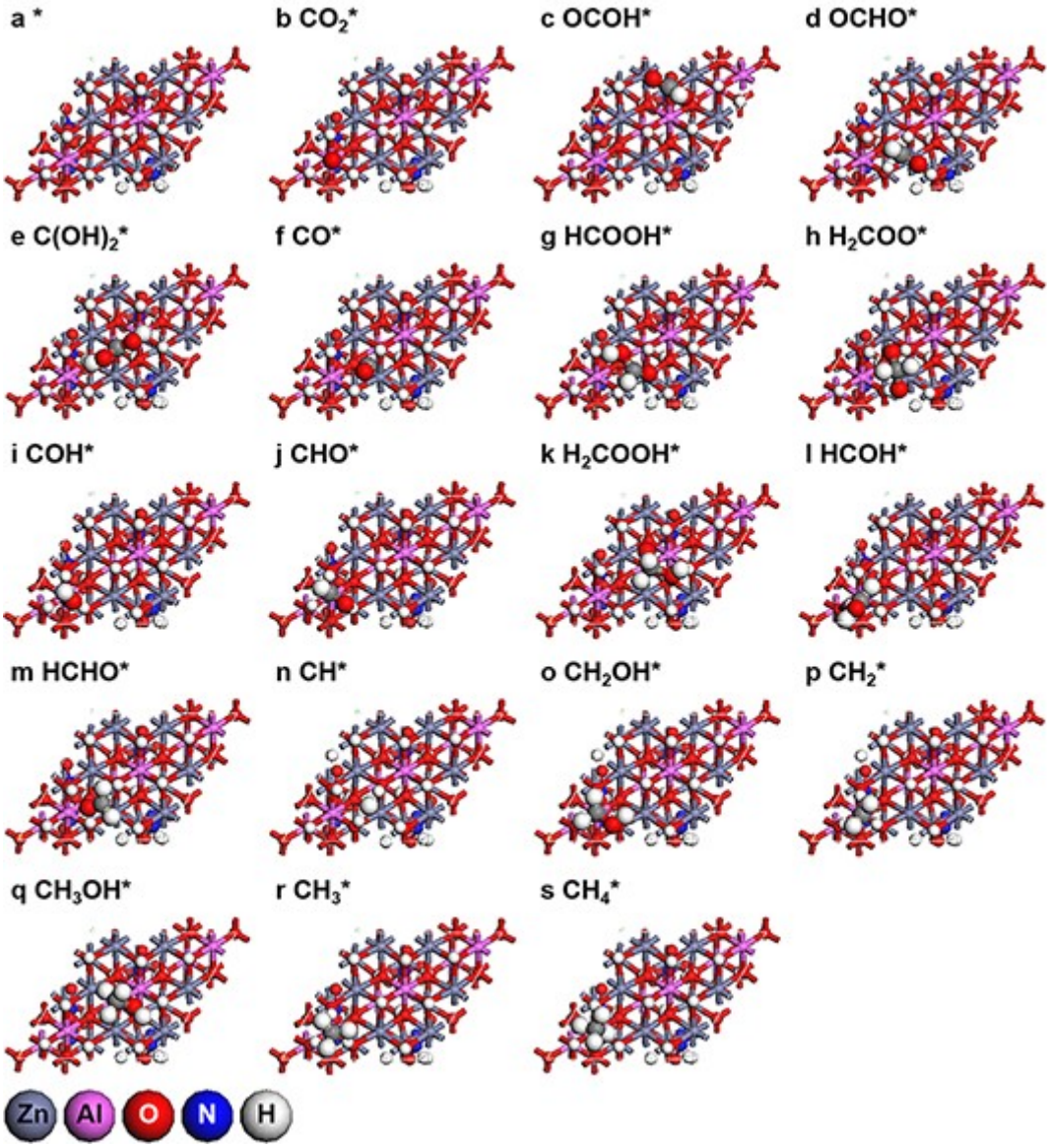

Fig. S12 Optimized geometries of reaction intermediates during CO_2 reduction over Zn_2Al-NO_3-LDH: (a) *, (b) CO_2*, (c) OCOH*, (d) OCHO*, (e) $C(OH)_2$*, (f) CO*, (g) HCOOH*, (h) H_2COO*, (i) COH*, (j) CHO*, (k) H_2COOH*, (l) HCOH*, (m) HCHO*, (n) CH*, (o) CH_2OH*, (p) CH_2*, (q) CH_3OH*, (r) CH_3*, and (s) CH_4*, respectively. The color code of each element is displayed on the bottom.

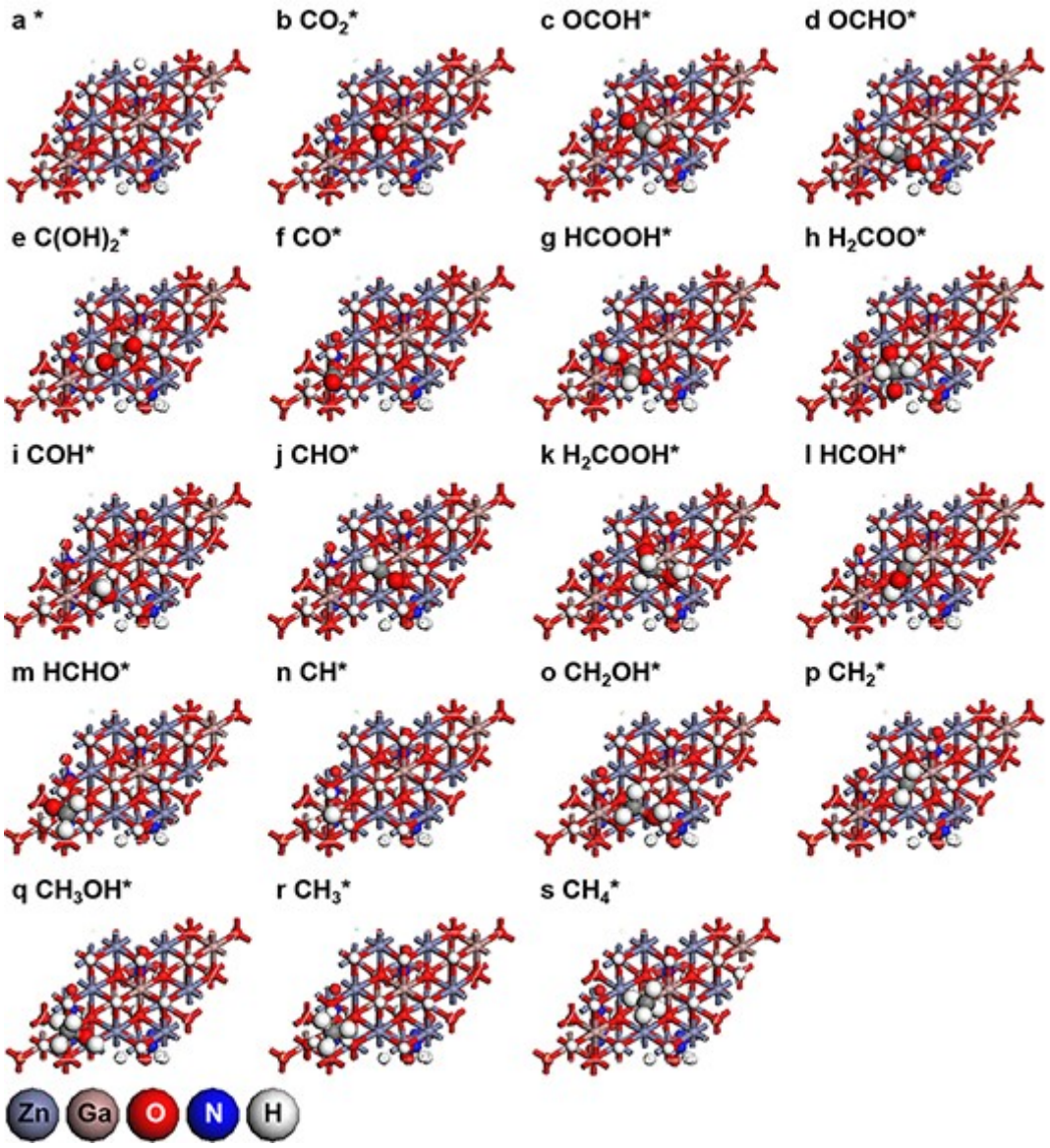

Fig. S13 Optimized geometries of reaction intermediates during CO_2 reduction over Zn_2Ga-NO_3-LDH: (a) *, (b) CO_2*, (c) OCOH*, (d) OCHO*, (e) $C(OH)_2$*, (f) CO*, (g) HCOOH*, (h) H_2COO*, (i) COH*, (j) CHO*, (k) H_2COOH*, (l) HCOH*, (m) HCHO*, (n) CH*, (o) CH_2OH*, (p) CH_2*, (q) CH_3OH*, (r) CH_3*, and (s) CH_4*, respectively. The color code of each element is displayed on the bottom.

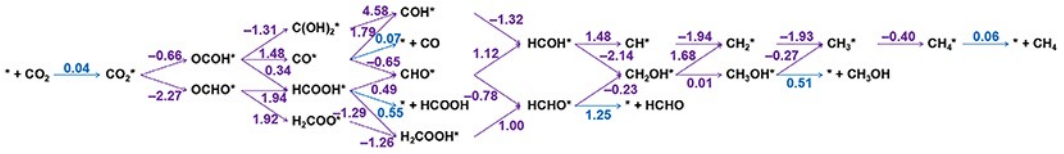

Fig. S14 Gibbs free energy changes (Δ*G*) of elementary steps in CO_2 reduction over Mg_2Ga-NO_3-LDH in the unit of eV. The condition is pH 0, 298.15 K, 0.1 MPa and without illumination.

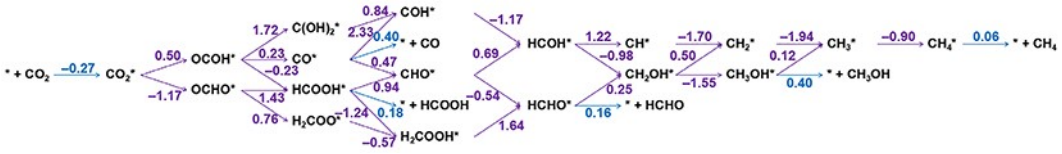

Fig. S15 Gibbs free energy changes (Δ*G*) of elementary steps in CO_2 reduction over Co_2Al-NO_3-LDH in the unit of eV. The condition is pH 0, 298.15 K, 0.1 MPa and without illumination.

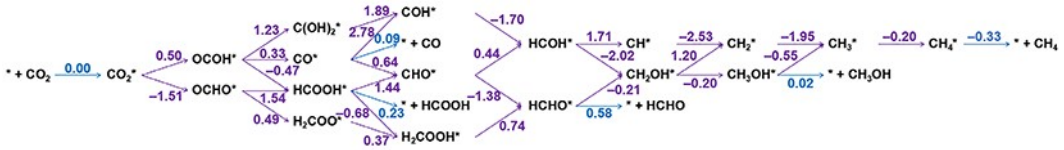

Fig. S16 Gibbs free energy changes (Δ*G*) of elementary steps in CO_2 reduction over Co_2Ga-NO_3-LDH in the unit of eV. The condition is pH 0, 298.15 K, 0.1 MPa and without illumination.

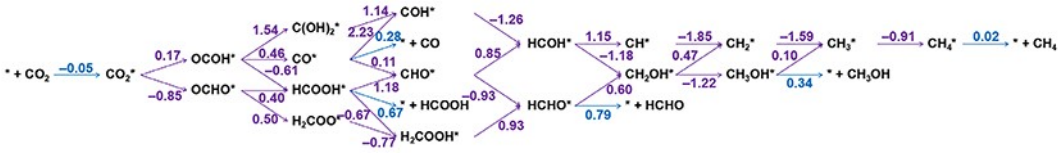

Fig. S17 Gibbs free energy changes (Δ*G*) of elementary steps in CO_2 reduction over Ni_2Al-NO_3-LDH in the unit of eV. The condition is pH 0, 298.15 K, 0.1 MPa and without illumination.

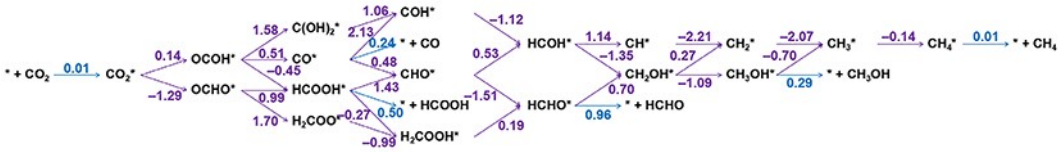

Fig. S18 Gibbs free energy changes (Δ*G*) of elementary steps in CO_2 reduction over Ni_2Ga-NO_3-LDH in the unit of eV. The condition is pH 0, 298.15 K, 0.1 MPa and without illumination.

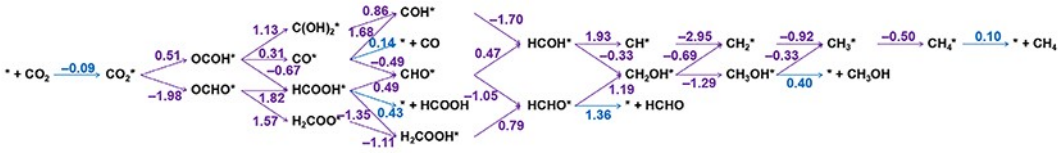

Fig. S19 Gibbs free energy changes (Δ*G*) of elementary steps in CO_2 reduction over Zn_2Al-NO_3-LDH in the unit of eV. The condition is pH 0, 298.15 K, 0.1 MPa and without illumination.

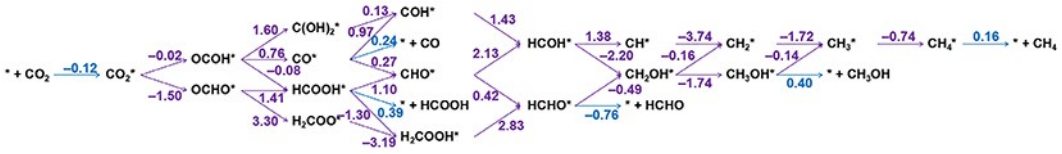

Fig. S20 Gibbs free energy changes (Δ*G*) of elementary steps in CO_2 reduction over Zn_2Ga-NO_3-LDH in the unit of eV. The condition is pH 0, 298.15 K, 0.1 MPa and without illumination.

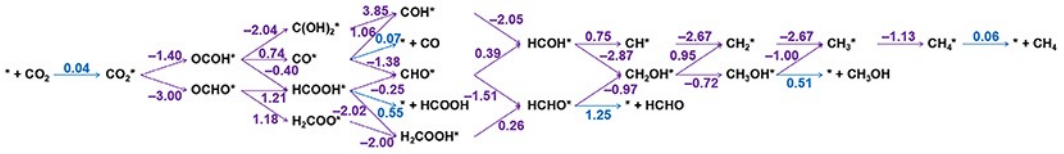

Fig. S21 Gibbs free energy changes (Δ*G*) of elementary steps in CO_2 reduction over Mg_2Ga-NO_3-LDH in the unit of eV. The condition is pH 7, 298.15 K, 0.1 MPa and with illumination.

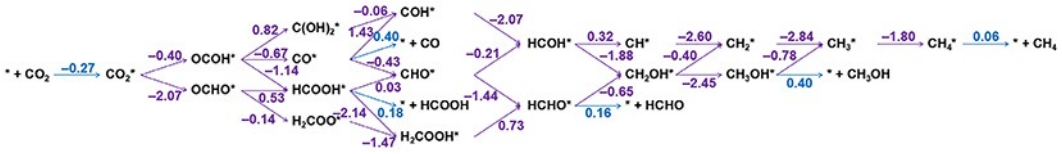

Fig. S22 Gibbs free energy changes (Δ*G*) of elementary steps in CO_2 reduction over Co_2Al-NO_3-LDH in the unit of eV. The condition is pH 7, 298.15 K, 0.1 MPa and with illumination.

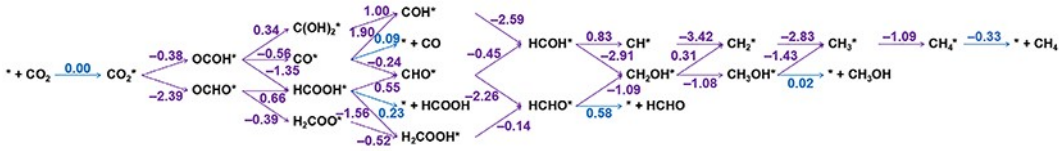

Fig. S23 Gibbs free energy changes (Δ*G*) of elementary steps in CO_2 reduction over Co_2Ga-NO_3-LDH in the unit of eV. The condition is pH 7, 298.15 K, 0.1 MPa and with illumination.

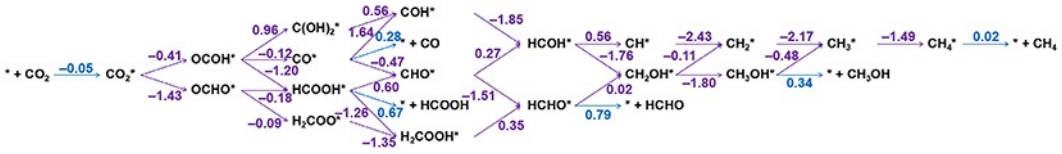

Fig. S24 Gibbs free energy changes (Δ*G*) of elementary steps in CO_2 reduction over Ni_2Al-NO_3-LDH in the unit of eV. The condition is pH 7, 298.15 K, 0.1 MPa and with illumination.

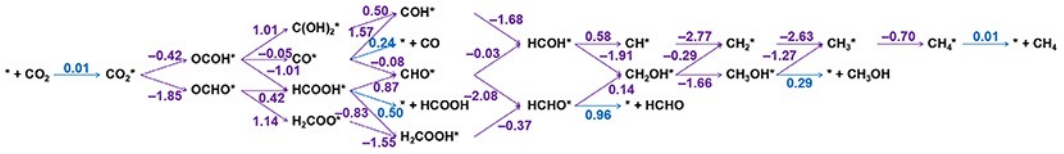

Fig. S25 Gibbs free energy changes (Δ*G*) of elementary steps in CO_2 reduction over Ni_2Ga-NO_3-LDH in the unit of eV. The condition is pH 7, 298.15 K, 0.1 MPa and with illumination.

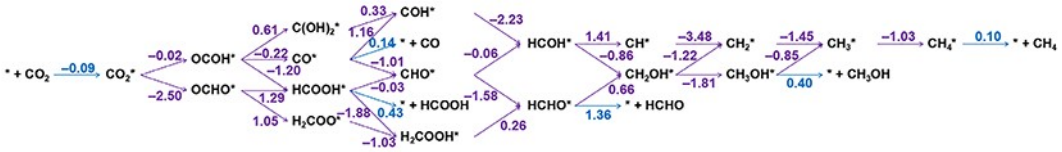

Fig. S26 Gibbs free energy changes (Δ*G*) of elementary steps in CO_2 reduction over Zn_2Al-NO_3-LDH in the unit of eV. The condition is pH 7, 298.15 K, 0.1 MPa and with illumination.

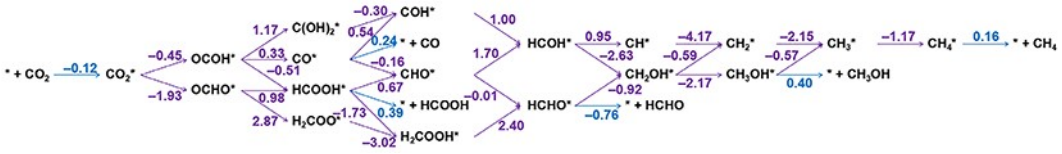

Fig. S27 Gibbs free energy changes (Δ*G*) of elementary steps in CO_2 reduction over Zn_2Ga-NO_3-LDH in the unit of eV. The condition is pH 7, 298.15 K, 0.1 MPa and with illumination.

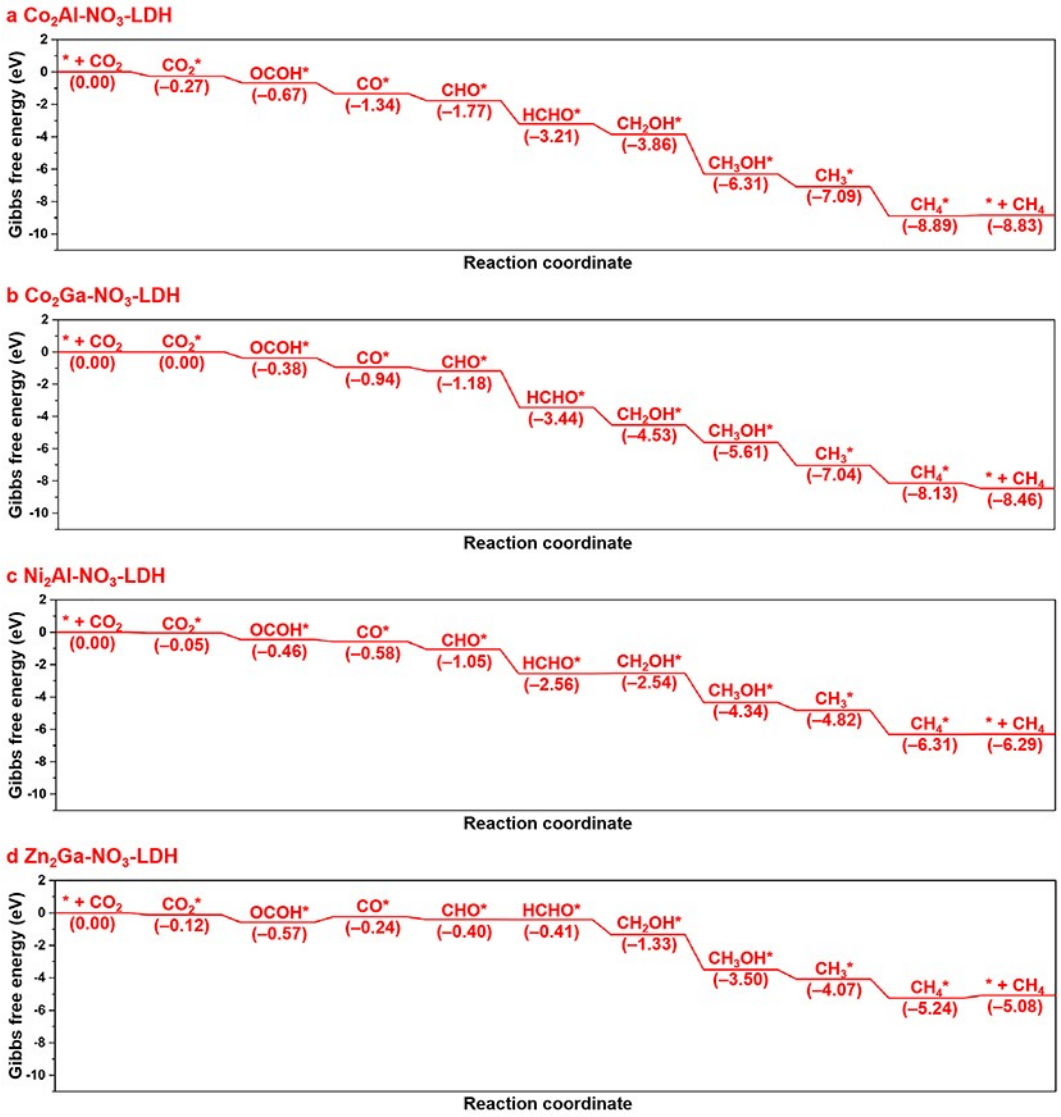

Fig. S28 Gibbs free energy diagrams of the main reaction pathways for photocatalytic CO_2 reduction over (a) Co_2Al-NO_3-LDH, (b) Co_2Ga-NO_3-LDH, (c) Ni_2Al-NO_3-LDH, and (d) Zn_2Ga-NO_3-LDH, respectively.

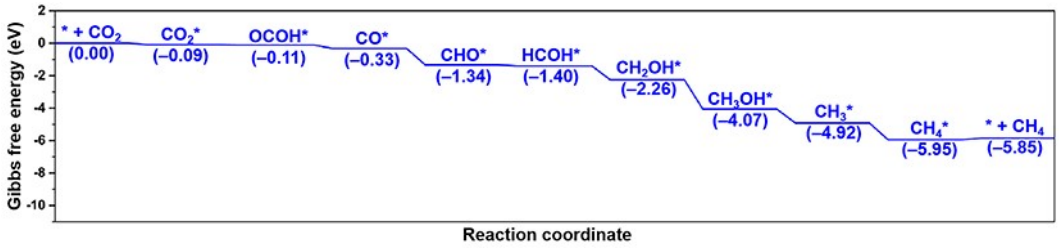

Fig. S29 Gibbs free energy diagrams of the main reaction pathways for photocatalytic CO_2 reduction over Zn_2Al-NO_3-LDH.

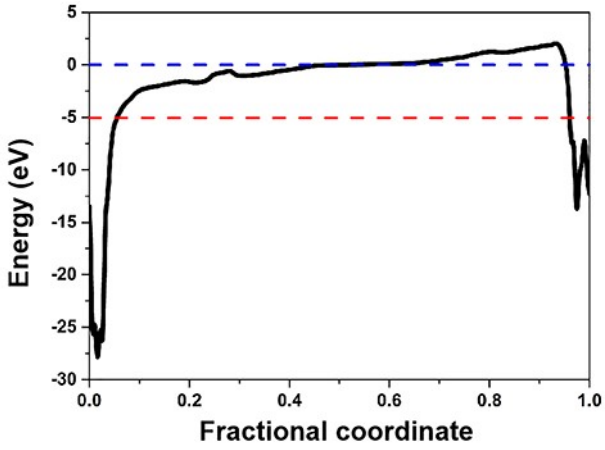

Fig. S30 Work functions of the (001) surface for $(ZnCu)_2Ga\text{-}NO_3$-LDH. Vacuum level (set as zero point) and Fermi level are labeled with dashed blue line and red line, respectively.

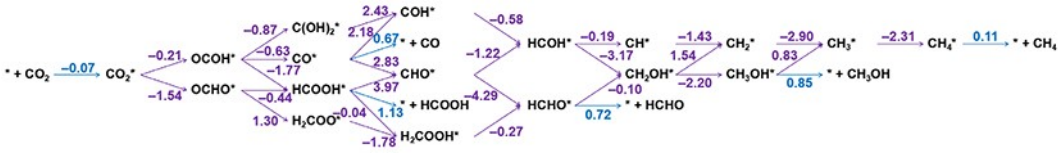

Fig. S31 Gibbs free energy changes (Δ*G*) of elementary steps in CO_2 reduction over $(ZnCu)_2Ga\text{-}NO_3$-LDH in the unit of eV. The condition is pH 7, 298.15 K, 0.1 MPa and with illumination.

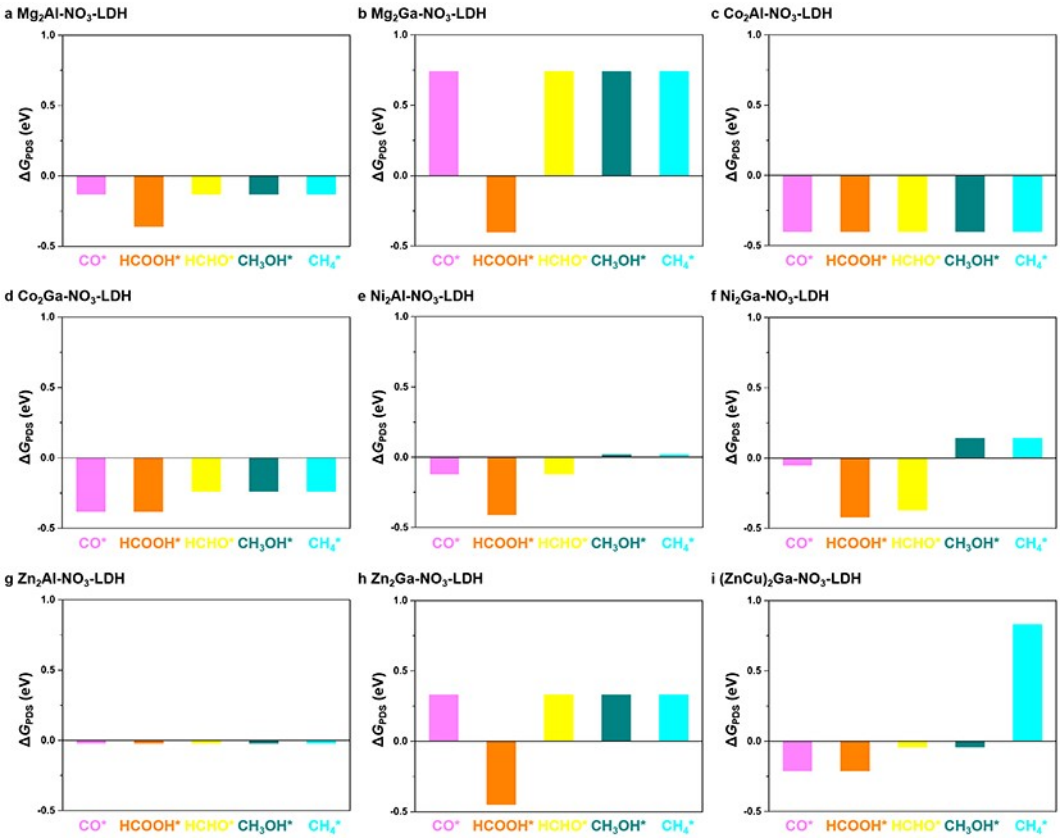

Fig. S32 ΔG_{PDS} for generating CO*, HCOOH*, HCHO*, CH_3OH*, and CH_4* under reaction condition of (a) Mg_2Al-NO_3-LDH, (b) Mg_2Ga-NO_3-LDH, (c) Co_2Al-NO_3-LDH, (d) Co_2Ga-NO_3-LDH, (e) Ni_2Al-NO_3-LDH, (f) Ni_2Ga-NO_3-LDH, (g) Zn_2Al-NO_3-LDH, (h) Zn_2Ga-NO_3-LDH, and (i) $(ZnCu)_2Ga$-NO_3-LDH.

Tables

Table S1 Experimental lattice parameters (*a*, *b*, and *c*) of M_2M'-NO_3-LDHs

Model	Lattice parameter (Å)					
	Experimental			Calculated		
	a	*b*	*c*	*a*	*b*	*c*
Mg_2Al-NO_3-LDH	3.05[S1]	3.05[S1]	8.79[S2]	3.02	3.03	8.78
Mg_2Ga-NO_3-LDH	3.09[S3]	3.09[S3]	8.79[S2]	3.05	3.08	8.89
Co_2Al-NO_3-LDH	3.09[S4]	3.09[S4]	8.79[S2]	3.03	3.04	8.64
Co_2Ga-NO_3-LDH	3.10[S5]	3.10[S5]	8.79[S2]	3.02	3.11	8.95
Ni_2Al-NO_3-LDH	3.05[S1]	3.05[S1]	8.79[S2]	3.00	3.03	8.87
Ni_2Ga-NO_3-LDH	3.08[S6]	3.08[S6]	8.79[S2]	3.04	3.06	8.84
Zn_2Al-NO_3-LDH	3.08[S1]	3.08[S1]	8.79[S2]	3.05	3.06	8.87
Zn_2Ga-NO_3-LDH	3.11[S7]	3.11[S7]	8.79[S2]	3.09	3.16	8.96

Table S2 Energies of CO_2 reduction intermediates at different adsorption sites of Mg_2Al-NO_3-LDH

Model	Energy (eV)		
	top	bridge	fcc
CO_2*	−38890.4470	−38890.4065	−38890.4337
OCOH*	−38906.8336	−38906.7778	−38906.6231
OCHO*	−38907.8194	−38908.1452	−38907.8902
$C(OH)_2$*	−38920.7460	−38920.5563	−38920.7002
CO*	−38452.3374	−38452.3221	−38452.3511
HCOOH*	−38922.5737	−38922.5089	−38922.5183
H_2COO*	−38922.3121	−38922.7157	−38922.6347
COH*	−38466.5764	−38466.6712	−38466.6790
CHO*	−38469.5116	−38469.7583	−38468.9898
H_2COOH*	−38939.8432	−38940.0609	−38939.6962
HCOH*	not converged	−38483.2064	not converged
HCHO*	−38485.5958	−38485.8926	−38485.8374
CH*	−38029.2951	−38029.5589	−38029.9054
CH_2OH*	−38502.1801	−38502.3360	−38502.3265
CH_2*	−38047.7712	−38046.9968	−38047.5121
CH_3OH*	−38518.2744	−38518.1256	−38518.2171
CH_3*	−38075.0703	−38075.2739	−38065.3595
CH_4*	−38082.1982	−38082.0234	−38081.9772

Table S3 Energies of CO_2 reduction intermediates at different adsorption sites of Mg_2Ga-NO_3-LDH

Model	Energy (eV)		
	top	bridge	fcc
CO_2*	−50856.4136	−50856.3946	−50856.3947
OCOH*	not converged	−50872.6165	not converged
OCHO*	−50873.9967	−50873.9400	−50873.7769
$C(OH)_2$*	−50886.8090	−50886.6332	−50886.7194
CO*	−50418.2934	−50418.2996	−50418.2924
HCOOH*	−50888.6118	−50888.6084	−50888.5967
H_2COO*	−50888.6052	−50888.6424	−50888.5583
COH*	−50432.4616	−50432.5101	−50432.4665
CHO*	−50435.3198	−50435.6443	−50434.8036
H_2COOH*	−50905.8388	−50905.7392	−50905.7133
HCOH*	not converged	not converged	not converged
HCHO*	−50451.7151	−50451.5607	−50451.7551
CH*	−49995.6147	−49995.6902	−49995.7483
CH_2OH*	−50468.1680	−50468.3246	−50468.3129
CH_2*	−50013.6855	−50013.3585	−50014.1222
CH_3OH*	−50484.3761	−50484.2608	−50484.3233
CH_3*	−50031.9517	−50032.0284	−50031.2464
CH_4*	−50048.0124	−50048.0117	−50047.9975

Table S4 Energies of CO_2 reduction intermediates at different adsorption sites of Co_2Al-NO_3-LDH

Model	Energy (eV)		
	top	bridge	fcc
CO_2*	−39665.2331	−39665.2346	−39665.2115
OCOH*	−39681.0485	−39681.2242	−39680.9187
OCHO*	−39682.2021	−39682.3024	−39681.9680
$C(OH)_2$*	−39695.3455	−39695.0108	−39695.3781
CO*	−39227.3984	−39227.4028	−39227.4084
HCOOH*	−39697.2282	−39696.8880	−39697.3786
H_2COO*	−39697.2475	−39697.7925	−39697.6048
COH*	−39240.7676	−39241.1512	−39241.1716
CHO*	−39243.6052	−39242.8935	−39242.8536
H_2COOH*	−39713.8353	−39714.1663	−39713.7418
HCOH*	−39258.0983	−39258.3035	−39257.9790
HCHO*	−39260.0983	−39260.0104	−39259.9918
CH*	−38803.4617	−38805.5095	−38804.0903
CH_2OH*	−39276.5555	−39275.1963	−39276.7322
CH_2*	−38822.3026	−38822.2657	−38821.8709
CH_3OH*	−39293.0070	−39292.6451	−39292.8131
CH_3*	−38840.3498	−38840.2521	−38840.5143
CH_4*	−38856.3248	−38856.8700	−38856.9296

Table S5 Energies of CO_2 reduction intermediates at different adsorption sites of Co_2Ga-NO_3-LDH

Model	Energy (eV)		
	top	bridge	fcc
CO_2*	–51623.3559	–51623.4618	–51623.5148
OCOH*	–51637.5067	not converged	–51637.4081
OCHO*	–51640.2971	–51640.4484	–51640.1589
$C(OH)_2$*	–51653.6100	–51653.5089	–51653.6932
CO*	–51185.6303	–51185.6648	–51185.6787
HCOOH*	–51655.2584	–51655.3190	–51655.4344
H_2COO*	–51655.9113	–51656.2597	–51656.3503
COH*	–51199.3545	–51199.4746	–51199.5358
CHO*	not converged	–51201.2261	–51201.1690
H_2COOH*	not converged	–51671.4452	–51671.4582
HCOH*	–51216.2032	not converged	–51216.5382
HCHO*	–51218.1285	–51218.4588	–51218.2720
CH*	–50762.2258	not converged	–50762.4936
CH_2OH*	–51234.7252	not converged	not converged
CH_2*	–50780.4599	not converged	not converged
CH_3OH*	–51251.0075	–51250.8517	–51251.0616
CH_3*	–50798.7906	not converged	not converged
CH_4*	–50815.1904	–50815.1148	–50815.1889

Table S6 Energies of CO_2 reduction intermediates at different adsorption sites of Ni_2Al-NO_3-LDH

Model	Energy (eV)		
	top	bridge	fcc
CO_2*	−43402.0431	−43402.0910	−43402.0484
OCOH*	−43418.4476	−43418.1125	−43417.7205
OCHO*	−43419.2565	−43419.3552	−43418.6013
$C(OH)_2$*	−43432.2258	−43432.1417	−43432.1411
CO*	−42964.2702	−42963.9394	−42964.1894
HCOOH*	−43434.3967	−43433.5941	−43433.5526
H_2COO*	−43433.6592	−43434.7847	−43434.5032
COH*	−42977.9547	−42978.1322	−42978.1743
CHO*	−42980.0729	−42979.8740	−42979.7848
H_2COOH*	−43450.5228	−43451.0619	−43451.0378
HCOH*	−42996.0821	−42994.9525	−42995.2125
HCHO*	−42996.8548	−42997.1137	−42997.1672
CH*	−42541.0676	−42541.1864	−42541.1504
CH_2OH*	−43014.0009	−43013.9833	−43012.8998
CH_2*	−42558.5712	−42559.3718	−42559.6508
CH_3OH*	−43029.8385	−43029.7277	−43029.5852
CH_3*	−42577.2406	−42577.8595	−42576.2270
CH_4*	−42593.6306	−42593.7421	−42593.6349

Table S7 Energies of CO_2 reduction intermediates at different adsorption sites of Ni_2Ga-NO_3-LDH

Model	Energy (eV)		
	top	bridge	fcc
CO_2*	−55359.9083	−55359.9504	−55359.9844
OCOH*	−55375.7676	−55376.5728	−55375.7600
OCHO*	−55376.6125	−55377.1770	−55376.6532
$C(OH)_2$*	−55390.1782	−55390.0319	−55390.1473
CO*	−54922.2316	−54922.2252	−54922.2470
HCOOH*	−55392.0768	−55391.9602	−55392.1973
H_2COO*	−55391.4731	−55392.7151	−55392.5573
COH*	−54935.9457	−54936.0885	−54935.7257
CHO*	−54939.0971	−54937.9025	−54937.9056
H_2COOH*	−55408.5235	−55408.8834	−55408.3682
HCOH*	−54953.8964	−54953.1540	−54952.8040
HCHO*	−54954.8848	−54955.2799	−54954.9641
CH*	−54499.0152	−54498.5798	−54499.0268
CH_2OH*	−54971.4913	−54971.9063	−54970.9757
CH_2*	−54517.0844	−54516.9653	−54516.8616
CH_3OH*	−54987.7009	−54987.6612	−54987.7425
CH_3*	−54535.2775	−54533.7893	−54534.5304
CH_4*	−54551.5870	−54551.5907	−54551.2964

Table S8 Energies of CO_2 reduction intermediates at different adsorption sites of Zn_2Al-NO_3-LDH

Model	Energy (eV)		
	top	bridge	fcc
CO_2*	–47686.2190	–47686.2425	–47686.2437
OCOH*	not converged	–47702.5056	not converged
OCHO*	–47703.5521	–47703.9425	–47703.5039
$C(OH)_2$*	–47716.5446	–47716.2900	–47716.4278
CO*	–47248.2149	–47248.2222	–47248.1564
HCOOH*	–47718.1824	–47718.2452	–47718.1887
H_2COO*	–47718.0436	–47718.2667	–47718.1942
COH*	–47262.0017	–47263.3856	–47262.4154
CHO*	–47265.5138	–47265.2938	–47264.4538
H_2COOH*	–47735.5253	–47735.4087	–47735.3934
HCOH*	–47280.3553	–47280.5120	–47280.5435
HCHO*	–47281.0395	–47281.3845	–47281.2813
CH*	–46825.2912	–46825.5819	–46825.2204
CH_2OH*	–47298.1772	not converged	–47296.6436
CH_2*	–46844.0468	–46844.1175	–46843.2050
CH_3OH*	–47314.0408	–47313.9965	–47314.0177
CH_3*	–46862.2165	–46862.2994	–46861.0456
CH_4*	–46877.8833	–46877.8737	–46877.8894

Table S9 Energies of CO_2 reduction intermediates at different adsorption sites of Zn_2Ga-NO_3-LDH

Model	Energy (eV)		
	top	bridge	fcc
CO_2*	−59645.1861	−59645.1591	−59645.1753
OCOH*	−59661.3859	−59661.2080	−59661.8666
OCHO*	−59662.1733	−59662.4024	−59662.3075
$C(OH)_2$*	−59675.4283	−59675.1398	−59675.3143
CO*	−59207.1197	−59207.1177	−59207.1572
HCOOH*	−59677.0530	−59677.2541	−59677.2522
H_2COO*	−59676.4597	−59676.9687	−59676.9465
COH*	−59220.8625	−59221.3697	−59221.3059
CHO*	−59223.0579	−59223.7235	−59223.4380
H_2COOH*	−59694.3044	−59694.1274	−59694.1259
HCOH*	−59237.7284	−59237.6510	−59237.7072
HCHO*	−59239.8865	−59240.2714	−59240.3621
CH*	−58783.9194	−58783.4883	−58784.0027
CH_2OH*	−59256.7859	−59257.2328	−59257.2052
CH_2*	−58802.4767	−58802.3483	−58801.2728
CH_3OH*	−59272.9040	−59272.8795	−59272.9678
CH_3*	−58820.5245	−58819.2209	−58819.8327
CH_4*	−58836.8482	−58836.8471	−58836.8229

Table S10 Energies of CO_2 reduction intermediates at different adsorption sites of $(ZnCu)_2Ga\text{-}NO_3$-LDH

Model	Energy (eV)		
	top	bridge	fcc
CO_2*	−59417.6124	−59417.6372	−59417.6800
OCOH*	not converged	not converged	−59433.8462
OCHO*	−59434.4482	−59434.6726	−59434.6151
$C(OH)_2$*	−59447.9759	−59448.6177	−59449.6726
CO*	not converged	−58980.3462	−58979.8378
HCOOH*	−59449.7771	−59450.5387	−59449.8168
H_2COO*	−59448.7444	−59449.2893	−59449.2030
COH*	−58993.6017	−58993.6996	−58993.6573
CHO*	−58996.5901	−58995.3117	−58995.2977
H_2COOH*	−59466.3900	−59466.3943	not converged
HCOH*	not converged	−59010.7624	not converged
HCHO*	−59012.6075	−59012.7731	−59012.6765
CH*	not converged	−58556.6257	−58556.4829
CH_2OH*	−59029.1222	−59029.2785	not converged
CH_2*	−58574.2100	−58574.5565	−58574.2071
CH_3OH*	−59046.0342	−59045.3992	−59045.4965
CH_3*	not converged	−58591.4990	−58593.2393
CH_4*	−58609.2886	−58609.3307	−58609.3577

References

S1 A. Dias, L. Cunha and A. C. Vieira, Synthesis and properties of $A_6B_2(OH)_{16}Cl_2{\cdot}4H_2O$ (A = Mg, Ni, Zn, Co, Mn and B = Al, Fe) materials for environmental applications, *Mater. Res. Bull.*, 2011, **46**, 1346–1351.

S2 F. Cavani, F. Trifiro and A. Vaccari, Hydrotalcite-type anionic clays: preparation, properties and applications, *Catal. Today*, 1991, **11**, 173–301.

S3 U. Unal, Short-time hydrothermal synthesis and delamination of ion exchangeable Mg/Ga layered double hydroxides, *J. Sol. State Chem.*, 2007, **180**, 2525–2533.

S4 Z.-P. Liu, R.-Z. Ma, M. Osada, N. Iyi, Y. Ebina, K. Takada and T. Sasaki, Synthesis, anion exchange, and delamination of Co-Al layered double hydroxide: assembly of the exfoliated nanosheet/polyanion composite films and magneto-optical studies, *J. Am. Chem. Soc.*, 2006, **128**, 4872–4880.

S5 X. Chen, H. Chai, Y. Cao, W. Zhou, Y. Li and Y. Yang, Hierarchical CoGa layered double hydroxides grown on nickel foam as high energy density hybrid supercapacitor, *Chem. Eng. J.*, 2020, **381**, 122620.

S6 A. Alvarez, R. Trujillano and V. Rives, Differently aged gallium-containing layered double hydroxides, *Appl. Clay Sci.*, 2013, **80–81**, 326–333.

S7 G. S. Thomas and P. V. Kamath, The layered double hydroxide (LDH) of Zn with Ga: synthesis and reversible thermal behaviour, *Solid State Sci.*, 2006, **8**, 1181–1186.